arXiv:1703.10814v1 [cond-mat.supr-con] 31 Mar 2017

Interface-Driven Two-Dimensional Superconductivity in Bilayers of $BaBiO_3$ and $BaPbO_3$

B. Meir, S. Gorol, T. Kopp, and G. Hammerl
Experimental Physics VI
Center for Electronic Correlations and Magnetism,
Institute of Physics, University of Augsburg,
86135 Augsburg, Germany
(Dated: April 3, 2017)

Besides the cuprate superconductors lead-doped barium bismuthate still attracts intense interest concerning its relatively high critical temperature and the nature of its superconductivity in vicinity to a charge density wave ordered topological insulator. Here we present bilayers of barium bismuthate and barium leadate and find two-dimensional superconductivity at their interfaces well described by current-voltage characteristics compatible with a Berezinskiĭ-Kosterlitz-Thouless transition. Magneto-transport studies independently prove the two-dimensional character of the superconducting properties in these bilayers. The particular dependence of the superconducting transition temperature on the thickness of the barium leadate top layer suggests the formation of the superconducting state to be strain-induced through the interface.

Interfaces in oxide heterostructures serve as an inexhaustible source for the creation of new electronic phases well constrained on the nanoscale [1]. Specifically, superconductivity confined to an interface is of particular importance not only because it is easy to tune by external fields but especially because the interface electron system results from an electronic reconstruction in dependence on bulk states with their versatile ground states [2–5]. The interface electron structure is controlled by bulk materials properties but also by the symmetry breaking at the edge of the respective bulk materials. The prominent oxide heterostructure of the two band insulators $SrTiO_3$ (STO) and $LaAlO_3$ (LAO) hosts such an interface-confined electron liquid [6–8] showing two-dimensional (2D) superconductivity at temperatures below $\approx 300\,\mathrm{mK}$ [9, 10]. Structural inversion symmetry breaking at the interface introduces a sizable Rashba spin-orbit coupling [11]. Also cuprate bilayers present striking features of their superconducting states: a high-T_c state confined to 2–3 nm is formed between insulating La_2CuO_4 and metallic $La_{1.55}Sr_{0.45}CuO_4$ [12], both of them not superconducting. Moreover, heterostructures built from the insulating oxides $CaCuO_2$ and STO allow for a superconducting interface [13].

Up to now, only few superconducting oxide interfaces have been realized. However it is an appealing challenge to identify further superconducting bilayers because different perovskite parent compounds account for novel characteristics of electronic states in proximity to the interface. For example, $BaBiO_3$ (BBO) is predicted to be a large-energy gap topological insulator due to spin-orbit coupling (when electron doped) [14], whereas the related compound $BaPbO_3$ (BPO) is a bulk metal [15]. In fact, both BBO and BPO are expected to preserve a "hidden" topological insulator phase when electron or hole doped [16, 17]. Moreover, lead-doped bulk BBO is well-known to be superconducting [18]. That finding now incites the question of whether the interface between BBO and BPO is a 2D superconductor. If this is the case, do the topological surface states generate Majorana fermions [19] and is that modulated with the Berezinskiĭ-Kosterlitz-Thouless (BKT) transition which by itself is topologically driven? The potential realization of topologically protected edge states is certainly a strong motivation to explore the interfacial electronic system of BBO/BPO in detail, although here we keep our focus exclusively on establishing the formation of a 2D superconducting phase in bilayers of BBO and BPO.

BBO crystallizes at room and low temperatures in perovskite related monoclinic structures [20]. The underlying octahedral distortion leads to symmetric breathing-mode displacements forcing the Bi^{3+} and Bi^{5+} ions to distinct crystal sites forming a bond-order charge density wave (CDW) [21–24]. The charge-ordered state can be altered by, e. g., substituting the metal cations in BBO giving rise to tremendeous changes in the structural and electronic properties of this very special perovskite: in homogeneosly doped bulk samples of $BaBi_{1-x}Pb_xO_3$ (BBPO) three-dimensional superconductivity is observed for doping ranges of $0.65 < x < 0.95$ with a maximum superconducting transition temperature of $T_c \approx 13\,\mathrm{K}$ for x near 0.75 [25–29]. The onset of superconductivity is attributed to the formation of a bimorphic phase consisting of orthorhombic and tetragonal polymorphs in BBPO [28–31]. By substituting barium by potassium, bulk samples of $Ba_{1-x}K_xBiO_3$ yield maximum critical temperatures of $T_c \approx 30\,\mathrm{K}$ for a potassium concentration of $x = 0.4$ [32]. The high-T_c superconductivity of these compounds was recently linked to correlation-enhanced electron-phonon coupling [33]. After the discovery of superconductivity in bulk samples, thin films of BBPO were soon realized by different growth techniques including sputtering [34–36] and pulsed laser deposition (PLD) [37].

Inspired by the discovery of a superconducting state at LAO/STO interfaces, we investigated BBO/BPO bilayers (BLs) in expectation to identify 2D superconductivity non-existent in both parent compounds. Thin films of nominal $BaBi_{0.25}Pb_{0.75}O_3$, BBO, BPO, and BBO/BPO BLs were grown by PLD using commercially available, stoichiometric targets with purities of at least 99.9% at maximum reachable density. We used single crystalline (001) oriented STO crystals as substrates, which we cleansed in acetone and isopropyl prior to deposition. HF buffering STO substrates [38, 39] had no significant impact on the results. The deposition temperatures were ≈ 635℃ for $BaBi_{0.25}Pb_{0.75}O_3$ thin films and ≈ 552℃ for BBO, BPO thin films and BBO/BPO BLs controlled by laser-heating and monitored by pyrometers. The background pressure of pure oxygen was kept mass-flow controlled at ≈ 1 mbar during growth. Our PLD system is equipped with a KrF laser having a fluency of $\approx 2\,\mathrm{J/cm^2}$. We used laser pulse energies in the range of 550–750 mJ and laser pulse frequencies of 3–5 Hz. After deposition the samples were cooled to ≈ 400℃ within three minutes and annealed at a background pressure of oxygen of ≈ 400 mbar for at least 17 minutes before the vacuum chamber was evacuated again.

For $BaBi_{0.25}Pb_{0.75}O_3$ thin films we used 1000 laser pulses (LP) resulting in film thicknesses of ≈ 420 nm. For thin films of BBO and BPO we used 50–150 LP corresponding to film thicknesses of ≈ 25–75 nm for BBO and ≈ 17–50 nm for BPO. Concerning the BBO/BPO BLs we kept the thickness of the BBO starting layer constant (always 100 LP) and only varied the number N of LP of the BPO top layer.

All grown $BaBi_{0.25}Pb_{0.75}O_3$ thin films show an increase in resistance with decreasing temperature and a superconducting transition at $T_{\mathrm{c,ip}} \approx 8$ K, which is determined at the inflection point (ip) of $R(T)$ at the transition (see Fig. 1, blue filled triangles facing right).

BBO and BPO thin films display peaks consistent with only $(00l)$ oriented planes in routinely taken x-ray diffraction (XRD) experiments. BBO thin films are insulating with resistances ranging from MΩ to GΩ over the whole accessible temperature range. Pure BPO thin films instead turn out to be metallic (see Fig. 1, gray hexagons).

BBO/BPO BLs reveal only peaks classified by $(00l)$ orientation in XRD studies separated in individual reflexes for BBO and BPO, respectively. Peaks assigned to a homogeneously doped $BaBi_{1-x}Pb_xO_3$ phase could not be identified (see Supplemental Material [40], Fig. S1). BLs with $N = 30$ are semiconducting at all accessible temperatures, BLs with $N = 40$ show semiconductor-to-superconductor transitions with $T_{\mathrm{c,ip}} \approx 3.0$ K (see Fig. 1, pink filled squares). An increase of the BPO thickness ($N = 60$) shifts the superconducting transition temperature to values as high as $T_{\mathrm{c,ip}} = 3.5$ K (see Fig. 1, red diamonds). Interestingly, with further increase of N we observe a dramatic reduction of the critical temperature

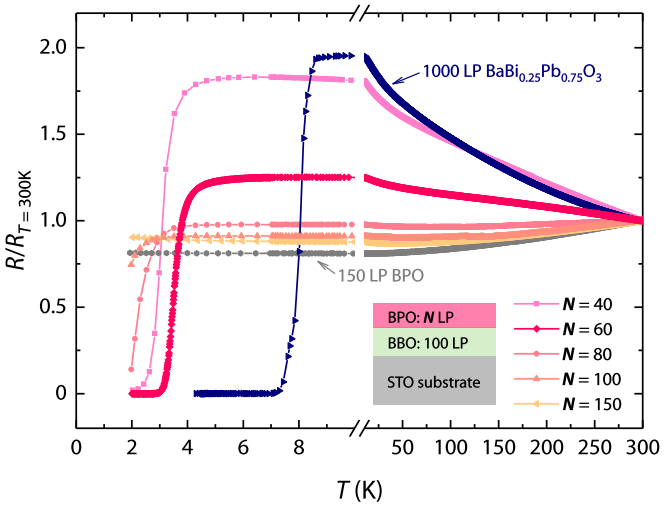

FIG. 1. Normalized resistances of pulsed laser deposition (PLD) grown thin films of $BaPbO_3$ (BPO) and $BaBi_{0.25}Pb_{0.75}O_3$ and $BaBiO_3$ (BBO)/BPO bilayers (BLs) as function of temperature. Whereas BBO thin films are highly insulating (not shown), BPO thin films show metallic behaviour (gray hexagons). Thin films of nominal $BaBi_{0.25}Pb_{0.75}O_3$ are superconducting at low temperatures. BLs with a fixed thickness of BBO (100 laser pulses (LP)) and variable thickness of BPO top layer (controlled by the number of LP N) undergo superconducting transitions (samples with $N = \{40, 60, 80, 100\}$).

($N = \{80, 100\}$) and no superconducting transition for samples with $N = 150$. The observation of an optimal BPO thickness to reach maximum T_{c} and the suppression of superconductivity beyond this thickness indicates that the BL superconductivity is related to the interface (see below) and may also be dependent on the thickness of the BBO starting layer (in the case of atomically thin BBO layers which is not investigated here).

If the superconducting transition is really driven by the interface, then a likely scenario is that a 2D superconducting sheet is formed within the bilayered samples. Such behavior is described by a BKT transition [41–44]. A convenient experimental method to characterize the transition into the algebraically ordered state is the familiar progression of current-voltage (IV) characteristics taken at temperatures around T_{c}: the applied voltage V breaks vortex-antivortex pairs and yields at $T = T_{\mathrm{BKT}}$ the well-known $V = I^{\alpha}$ behavior with $\alpha = 3$, whereas the current I responds linear in V for a state with free vortices above T_{BKT} [45]. A direct validation of this observation can be made by analyzing the $R(T)$ dependence. For a BKT transition, the resistance follows $R \propto R_{\mathrm{n}} \exp(-b/\sqrt{t})$ [43] near T_{BKT} with b being a material parameter in the order of unity [45] and $t = T/T_{\mathrm{BKT}} - 1$. Our data yield $b = 1.22$ and $T_{\mathrm{BKT}} = 3.26$ K matching the value $T_{\mathrm{BKT}} = 3.19$ K obtained independently from the IV measurements (see Supplemental Material [40], Fig. S2). The perfect agreement of our results (see Fig. 2) with the

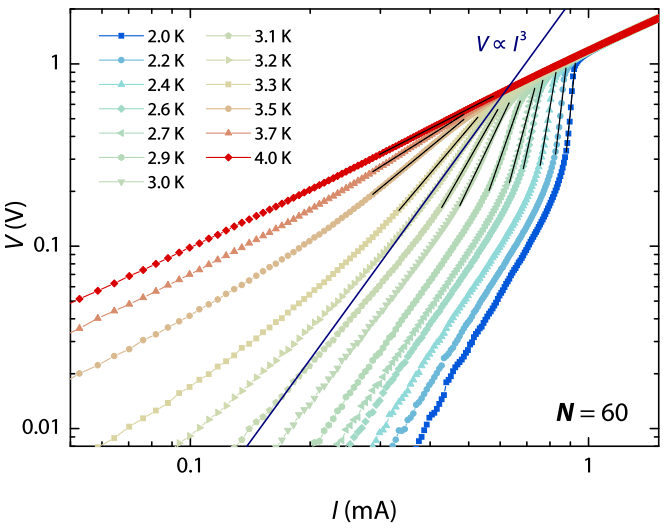

FIG. 2. Measured current-voltage (IV) characteristics of a BBO/BPO BL ($N = 60$) at temperatures ranging from 2 K (blue) to 4 K (red). Straight black lines are polynomial fits following the measured data directly at the transition. At 3.2 K the IV curve is best represented by a cubic fit (straight blue line) identifying 2D superconductivity following a Berezinskiĭ-Kosterlitz-Thouless (BKT) transition. The deviation of the fit for small currents is attributed to finite size effects [46].

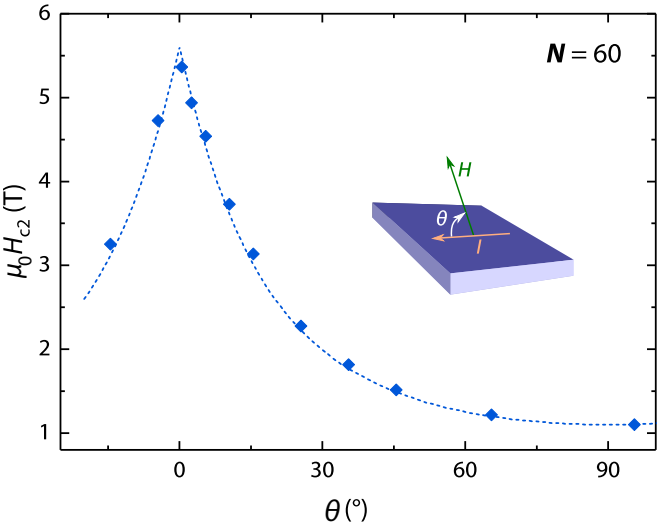

FIG. 3. Observed dependence of the upper critical magnetic field H_{c2} of a superconducting BL ($N = 60$) on the direction θ of the externally applied swept magnetic field (filled diamonds). The data are well represented by Eq. (1) (dashed line) which applies to a 2D superconducting sheet in the GL regime [49, 50] with $H_{c2,\parallel} = 5.6\,\mathrm{T}$ and $H_{c2,\perp} = 1.1\,\mathrm{T}$.

BKT predictions signifies unambiguously that indeed a 2D superconducting sheet is formed through the interface. The ohmic regime observed below T_{BKT} for small currents is attributed to be responsible for the deviations from the fits due to finite size effects [46].

An estimate of the thickness of the superconducting sheet can be retrieved by measuring the magneto-transport properties of our BLs. Such measurements are evaluated in the Ginzburg-Landau (GL) regime for magnetic fields up to H_{c2}. They also act as an independent proof for the observed 2D superconductivity given that the sheet thickness d_{sc} is comparable to or smaller than the GL coherence length ξ_{GL} [47, 48]. Fig. 3 exemplarily summarizes the observed dependence of the upper critical magnetic field H_{c2} of a BL with $N = 60$ on the angle θ, in respect to the sample plane of the externally applied swept magnetic field. As expected for a 2D superconductor the in-plane field $H_{c2,\parallel}$ ($\theta = 0°$) is much higher than the out-of-plane field $H_{c2,\perp}$ ($\theta = 90°$). Following Tinkham's analysis [49–51] both magnetic fields can be experimentally determined on the basis of the relation:

$$\left|\frac{H_{c2}(\theta)\sin\theta}{H_{c2,\perp}}\right| + \left(\frac{H_{c2}(\theta)\cos\theta}{H_{c2,\parallel}}\right)^2 = 1. \qquad (1)$$

The GL theory for thin superconducting sheets allows to express both magnetic fields in terms of the magnetic flux quantum ϕ_0, the thickness d_{sc} of the 2D superconducing sheet, the product of the penetration depth and the thermodynamic critical field [52]. Eliminating last said quantity the thickness d_{sc} can be calculated [51] with the help of experimentally obtained values of $H_{c2,\parallel}$ and $H_{c2,\perp}$ via

$$d_{\mathrm{sc}} = \sqrt{\frac{6\phi_0 H_{c2,\perp}}{\pi H_{c2,\parallel}^2}}, \qquad (2)$$

supporting a thickness of the 2D superconducting sheet to be in the range of $d_{\mathrm{sc}} \approx 11.8\,\mathrm{nm}$ being clearly smaller than the nominal thickness of the BPO top layer. The calculated thickness d_{sc} is robust against different experimental determination of H_{c2} (see Supplemental Material [40], Fig. S3). In contrast, d_{sc} of a nominal $BaBi_{0.25}Pb_{0.75}O_3$ thin film (60 LP) is of the same size as the overall thickness of the thin film (see Supplemental Material [40], Fig. S4).

The coherence length of the BL ($N = 60$) is estimated to be $\xi_{\mathrm{GL}} \approx 11.0\,\mathrm{nm}$, the value of which we extracted from the temperature dependence of the upper critical magnetic field obtained from $R(T, H)$ measurements (see Supplemental Material [40], Fig. S5). This is consistent with the prerequisites of the GL theory [47].

We suggest that the occurrence of 2D superconductivity in BBO/BPO BLs results from a strained growth of BPO on top of BBO possibly also affecting the crystallographic phase of BBO at the interface. Reciprocal space maps, which were taken for BLs with $N = 50$ and $N = 150$ (see Fig. 4a and 4b), prove that BBO grows epitaxially and fully relaxed on STO substrates consistent with domain-matched expitaxy [53, 54]. BPO however grows strained on top of BBO for thin layers ($N = 50$, Fig 4a) and relaxes more and more for thicker

layers ($N = 150$, Fig. 4b). We studied the strain effect in more detail in XRD $\theta/2\theta$ measurements taken for several BLs with different N (see Fig. 4c). With increasing N the 2θ position of the (004) peak of BPO shifts towards larger angles supporting a relaxation of interface-induced strain in the on-growing lattice of BPO. For BLs with $N = \{80, 100, 150\}$ the peak position of BPO stabilizes serving as an indication for reaching a relaxed state.

These observations aid the idea of a strain-only effect at the interface: as BLs with $N = 50$ become superconducting, whereas those with $N = 150$ stay metallic in the accessible temperature range, a possible existence of an established homogeneously doped region equal to $BaBi_{1-x}Pb_xO_3$ is hardly conceivable. Ultimately a most favorable thickness of the BPO film exists to assign a robustly induced superconducting phase with maximum T_c.

In this study we have shown that BLs of BBO and BPO become superconducting depending on the thickness of the BPO top layer with transition temperatures as high as $T_{c,ip} = 3.5\,K$ for our given sample layout. The electrical transport characterization clearly revealed a BKT transition identifying a 2D superconducting state within the BLs. Magneto-transport investigations independently provide evidence for the two-dimensionality of the superconducting sheet estimating the thickness of the sheet to be $d_{sc} \approx 11.8\,nm$. X-ray studies suggest an interface-driven epitaxial-matched strain effect at the interface between BBO and BPO responsible for the occurrence of the observed 2D superconducting state. The encountered transition in BBO/BPO bilayers is a remarkable further precedent of interface driven ground-state variance. With the identification of a robust superconducting state at the interface of two "hidden" topological insulators [16] it will be compelling to determine the surface states of the superconducting sheet in future work.

We thank A. P. Kampf for helpful discussions. We thank S. Esser for helpful discussions and his support in the measurement and the evaluation of the data for the reciprocal space maps. This work was supported by the DFG through TRR 80.

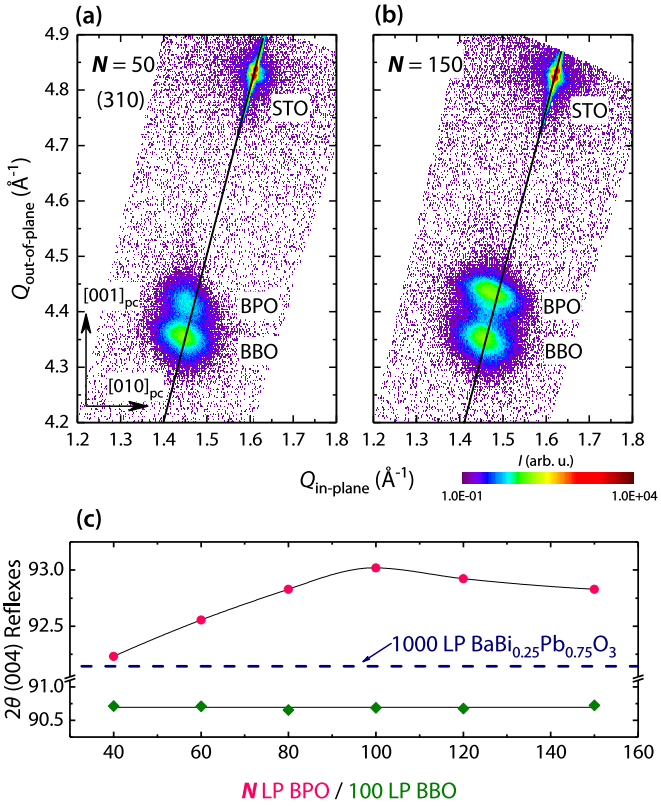

FIG. 4. XRD studies on BLs of BBO (100 LP)/BPO (N LP) grown on (001) oriented STO substrates. Reciprocal space maps of BLs for a) $N = 50$ (superconducting) and b) $N = 150$ (metallic). Whereas BBO grows completely relaxed on STO substrates following the relaxation line (black), the locations of both peaks of BPO are clear indicators for a strained growth of BPO on BBO. The observed shift of the BPO peak away from BBO peak for larger N supports the idea that superconductivity is strain-induced. c) Obtained (004) peak positions of BBO and BPO in BBO/BPO BLs from a series of $\theta/2\theta$ scans (black lines serve as guides to the eye). Whereas BBO shows no significant shift in its peak positions, the BPO peaks move to lower angles with decreasing N supporting ongoing strain-induced growth.

[1] J. Mannhart and D. G. Schlom, Science **327**, 1607 (2010).
[2] R. Hesper, L. H. Tjeng, A. Heeres, and G. A. Sawatzky, Phys. Rev. B **62**, 16046 (2000).
[3] S. Okamoto and A. J. Millis, Nature **428**, 630 (2004).
[4] In fact, Hesper, Tjeng, Heeres, and Sawatzky [2] coined the term *electronic reconstruction* in connection with the surface electronic structure associated with a polar surface termination. Here, we take the viewpoint of Okamoto and Millis [3] generalizing the term *electronic reconstruction* to include all situtations where the surface or interface electronic phase differs from that in the bulk component materials.
[5] P. Zubko, S. Gariglio, M. Gabay, P. Ghosez, and J.-M. Triscone, Annu. Rev. Condens. Matter Phys. **2**, 141 (2011).
[6] A. Ohtomo and H. Y. Hwang, Nature **427**, 423 (2004).
[7] A. Ohtomo and H. Y. Hwang, Nature **441**, 120 (2006).
[8] M. Breitschaft, V. Tinkl, N. Pavlenko, S. Paetel, C. Richter, J. R. Kirtley, Y. C. Liao, G. Hammerl, V. Eyert, T. Kopp, et al., Phys. Rev. B **81**, 153414 (2010).
[9] N. Reyren, S. Thiel, A. D. Caviglia, L. Fitting Kourkoutis, G. Hammerl, C. Richter, C. W. Schneider, T. Kopp, A.-S. Rüetschi, D. Jaccard, et al., Science **317**, 1196 (2007).
[10] A. D. Caviglia, S. Gariglio, N. Reyren, D. Jaccard, T. Schneider, M. Gabay, S. Thiel, G. Hammerl, J. Mannhart, and J.-M. Triscone, Nature **456**, 624 (2008).
[11] A. D. Caviglia, M. Gabay, S. Gariglio, N. Reyren, C. Cancellieri, and J.-M. Triscone, Phys. Rev. Lett. **104**, 126803 (2010).

[12] A. Gozar, G. Logvenov, L. Fitting Kourkoutis, A. T. Bollinger, L. A. Giannuzzi, D. A. Muller, and I. Bozovic, Nature **455**, 782 (2008).

[13] D. Di Castro, C. Cantoni, F. Ridolfi, C. Aruta, A. Tebano, N. Yang, and G. Balestrino, Phys. Rev. Lett. **115**, 147001 (2015).

[14] B. Yan, M. Jansen, and C. Felser, Nature Phys. **9**, 709 (2013).

[15] H. Ikushima and S. Hayakawa, Solid Stat. Electr. **9**, 921 (1966).

[16] G. Li, B. Yan, R. Thomale, and W. Hanke, Nature Phys. **5**, 10435 (2015).

[17] Here, the term "hidden" is to be understood in the sense that the electronic structure displays a topological gap in the vicinity of the Fermi energy with a Dirac-type of topological surface state [16].

[18] A. W. Sleight, US Patent 3932315 (1974).

[19] L. Fu and C. L. Kane, Phys. Rev. Lett. **100**, 096407 (2008).

[20] A. W. Sleight, Physica C **514**, 152 (2015).

[21] D. E. Cox and A. W. Sleight, Solid State Commun. **19**, 969 (1976).

[22] D. E. Cox and A. W. Sleight, Acta Crys. Sec. B **35**, 1 (1979).

[23] C. M. Varma, Phys. Rev. Lett. **61**, 2713 (1988).

[24] H.-T. Kim, Phys. Rev. B **54**, 90 (1996).

[25] A. W. Sleight, J. L. Gillson, and P. E. Bierstedt, Solid. Stat. Commun. **17**, 27 (1975).

[26] T. D. Than, A. Koma, and S. Tanaka, Appl. Phys. **22**, 205 (1980).

[27] B. Batlogg, Physica **126B**, 275 (1984).

[28] E. Climent-Pascual, N. Ni, S. Jia, Q. Huang, and R. J. Cava, Phys. Rev. B **83**, 174512 (2011).

[29] P. Giraldo-Gallo, H. Lee, Y. Zhang, M. J. Kramer, M. R. Beasley, T. H. Geballe, and I. R. Fisher, Phys. Rev. B **85**, 174503 (2012).

[30] P. V. Balachandran and J. M. Rondinelli, Phys. Rev. B **88**, 054101 (2013).

[31] P. Giraldo-Gallo, Y. Zhang, C. Parra, H. C. Manoharan, M. R. Beasley, T. H. Geballe, M. J. Kramer, and I. R. Fisher, Nature Commun. **6**, 8231 (2015).

[32] R. J. Cava, B. Batlogg, J. J. Krajeski, R. Farrow, L. W. Rupp, A. E. White, K. Short, W. F. Peck, and T. Kometani, Nature **332**, 814 (1988).

[33] Z. P. Yin, A. Kutepov, and G. Kotliar, Phys. Rev. X **3**, 021011 (2013).

[34] L. R. Gilbert, R. Messier, and R. Roy, Thin Solid Films **54**, 129 (1978).

[35] M. Suzuki, T. Murakami, and T. Inamura, Jpn. J. Appl. Phys. **19**, L231 (1980).

[36] Y. Hidaka, M. Suzuki, T. Murakami, and T. Inamura, Thin Solid Films **106**, 311 (1983).

[37] S. V. Zaitsev-Zotov, A. N. Martynyuk, and E. A. Protasov, Sov. Phys. Solid State **25**, 100 (1983).

[38] M. Kawasaki, K. Takahashi, T. Maeda, R. Tsuchiya, M. Shinohara, O. Ishiyama, T. Yonezawa, M. Yoshimoto, and H. Koinuma, Science **266**, 1540 (1994).

[39] G. Koster, B. L. Kropman, G. J. H. M. Rijnders, D. H. A. Blank, and H. Rogalla, Appl. Phys. Lett. **73**, 2920 (1998).

[40] See Supplemental Material at ...

[41] V. L. Berezinskiĭ, Sov. Phys. JETP **32**, 493 (1971).

[42] V. L. Berezinskiĭ, Sov. Phys. JETP **34**, 610 (1972).

[43] J. M. Kosterlitz and D. J. Thouless, J. Phys. C: Solid State Phys. **6**, 1181 (1973).

[44] J. M. Kosterlitz, J. Phys. C: Solid State Phys. **7**, 1046 (1974).

[45] B. I. Halperin and D. R. Nelson, J. Low Temp. Phys. **36**, 599 (1979).

[46] K. Medvedyeva, B. J. Kim, and P. Minnhagen, Phys. Rev. B **62**, 14531 (2000).

[47] M. Tinkham, *Introduction to Superconductivity* (McGraw Hill, 1996).

[48] P. G. De Gennes, *Superconductivity of Metals and Alloys* (Westview Press, 1999).

[49] M. Tinkham, Phys. Rev. **129**, 2413 (1963).

[50] M. Tinkham, Phys. Lett. **9**, 217 (1964).

[51] F. E. Harper and M. Tinkham, Phys. Rev. **172**, 441 (1968).

[52] V. L. Ginzburg and L. D. Landau, Zh. Eksperim. i Teor. Fiz. **20**, 1064 (1950).

[53] T. Zheleva, K. Jagannadham, and J. Narayan, J. Appl. Phys. **75**, 860 (1994).

[54] J. Narayan and B. C. Larson, J. Appl. Phys. **93**, 278 (2003).

arXiv:1703.10814v1 [cond-mat.supr-con] 31 Mar 2017

SUPPLEMENTAL MATERIAL

Interface-Driven Two-Dimensional Superconductivity in Bilayers of $BaBiO_3$ and $BaPbO_3$

B. Meir, S. Gorol, T. Kopp, and G. Hammerl

Experimental Physics VI

Center for Electronic Correlations and Magnetism,

Institute of Physics, University of Augsburg,

86135 Augsburg, Germany

With this Supplemental Material we provide additional x-ray characterization of our samples and explicitly discuss the extraction of critical values such as the BKT transition temperature T_{BKT}, the upper critical magnetic fields $H_{\mathrm{c2},\perp}$ and $H_{\mathrm{c2},\parallel}$, the thickness of the superconducting sheet d_{sc}, and the GL coherence length ξ_{GL} from our measured data.

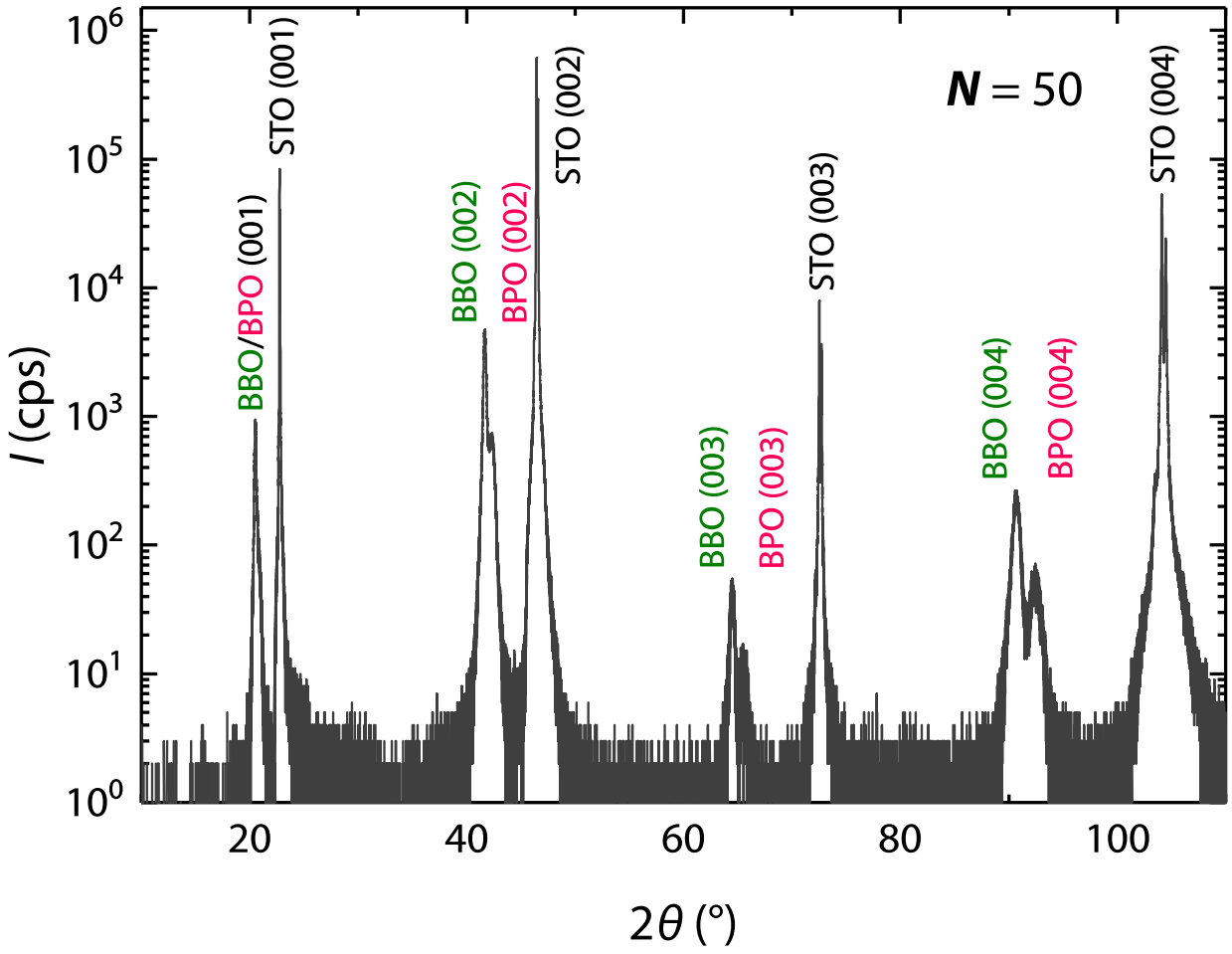

FIG. S1. Exemplary $\theta/2\theta$ scan obtained from a BBO/BPO BL with $N = 50$ (number of laser pulses) grown on (001) oriented STO substrate by PLD. The peaks assigned to BBO and BPO are well separated in individual reflexes at their characteristic positions, respectively. Peaks attributed to a homogeneously doped $BaBi_{1-x}Pb_xO_3$ phase can not be identified.

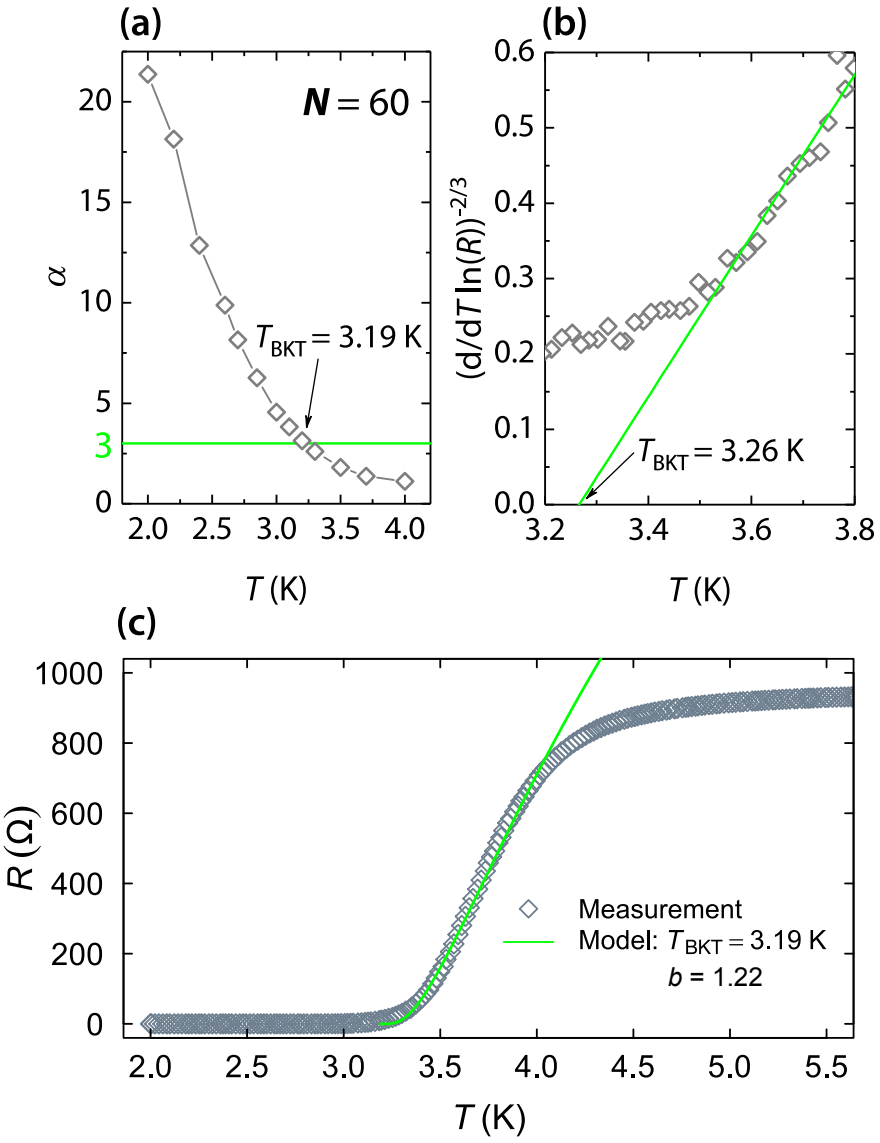

FIG. S2. Independent evaluation of T_{BKT} from current-voltage characteristics and the $R(T)$ dependence of a BBO/BPO BL with $N = 60$ (number of laser pulses). a) Obtained dependence of the exponent α taken from the IV measurements shown in Fig. 2 as a function of temperature. The BKT transition is identified where $\alpha = 3$ resulting in $T_{\mathrm{BKT}} = 3.19\,\mathrm{K}$. b) T_{BKT} can be retrieved from the $R(T)$ dependence where the resistance is described by $R \propto R_{\mathrm{n}} \exp(-b/\sqrt{t})$ with b being a material parameter in the range of unity and $t = T/T_{\mathrm{BKT}} - 1$. A fit to the data yields $T_{\mathrm{BKT}} = 3.26\,\mathrm{K}$. c) Direct evaluation of the $R(T)$ curve in terms of the standard BKT formalism yields $T_{\mathrm{BKT}} = 3.19\,\mathrm{K}$ and $b = 1.22$.

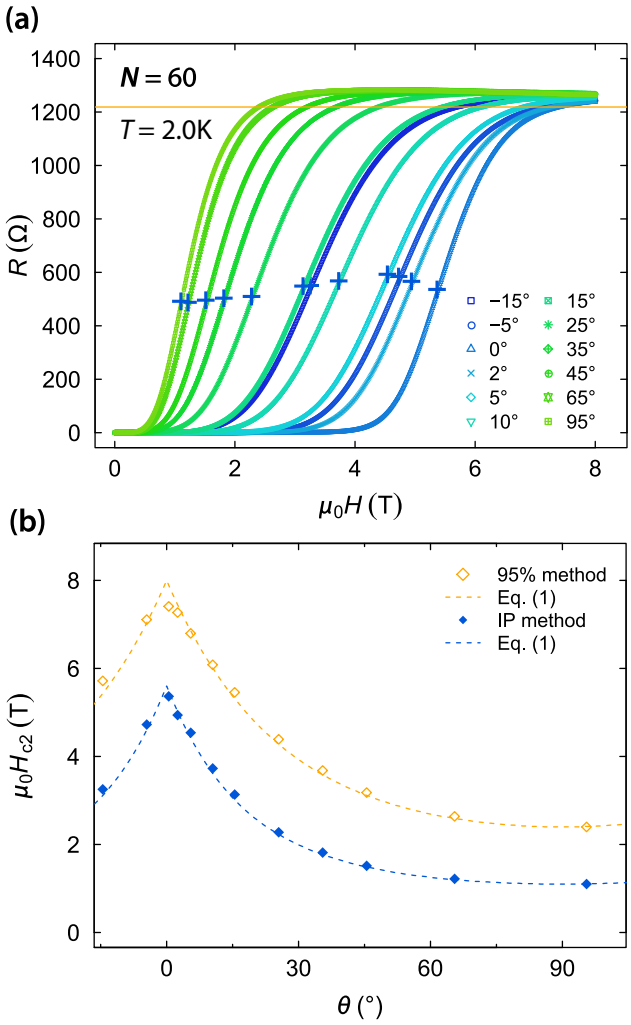

FIG. S3. Evaluation of H_{c2} from magneto-transport measurements taken at $T = 2.0\,\mathrm{K}$. a) Dependence of the resistance on the strength of an applied magnetic field in various orientations in respect to the sample plane. The value of H_{c2} is either retrieved by identifying the inflection point (IP) of the $R(H)$ dependence (blue crosses) or by reaching 95% of the normal-state resistance (indicated by the orange coloured line, in accordance with the evaluation given, e. g., in J. M. E. Geers, C. Attanasio, M B. S. Hesselberth, J. Aarts, and P H. Kes, Phys. Rev. B **63**, 094511 (2001)). b) Obtained dependence of the upper critical magnetic field H_{c2} as function of the angle θ of the applied swept magnetic field in respect to the sample plane for both evaluation methods described in a). The different values of $H_{c2,\parallel}$ and $H_{c2,\perp}$ extracted from both methods (using Equation (1)) result in values of d_{sc} being 11.8 nm (blue coloured) and 12.2 nm (orange coloured), respectively, proving the robustness of d_{sc} against different evaluations of the magneto-transport data.

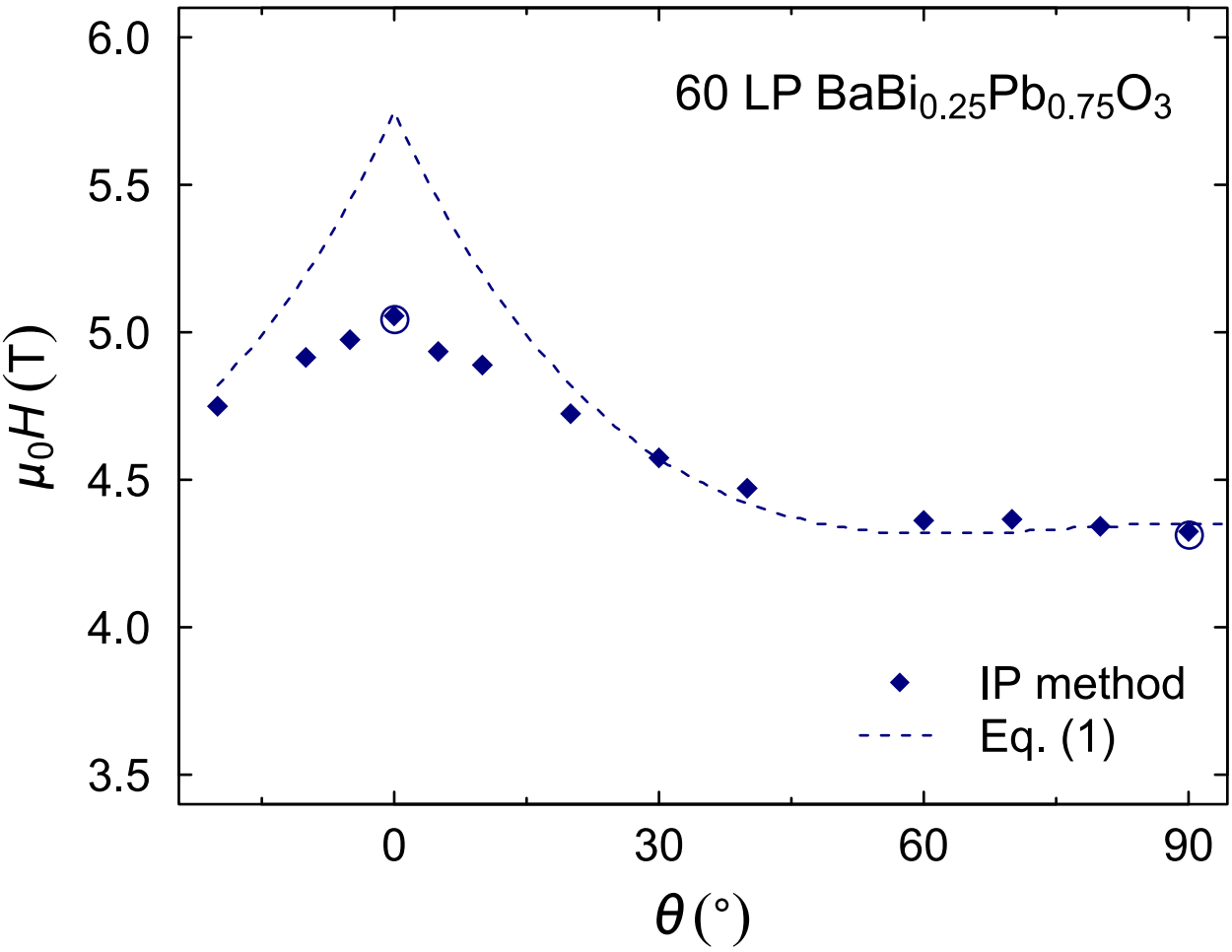

FIG. S4. Obtained dependence of the upper critical magnetic field as a function of the angle θ of the applied swept magnetic field in respect to the sample plane for a homogeneous doped $BaBi_{0.25}Pb_{0.75}O_3$ thin film grown by PLD with 60 LP and measured at $T = 2.0\,\mathrm{K}$. The data show a reduced influence of the magnetic field on the value of H_{c2} as expected for thicker films (see Ref. [51]). Extracted values (blue coloured, outlined circles) of $H_{c2,\parallel}$ and $H_{c2,\perp}$ result in $d_{sc} = 25.9\,\mathrm{nm}$ comparable to the film thickness of 24.7 nm.

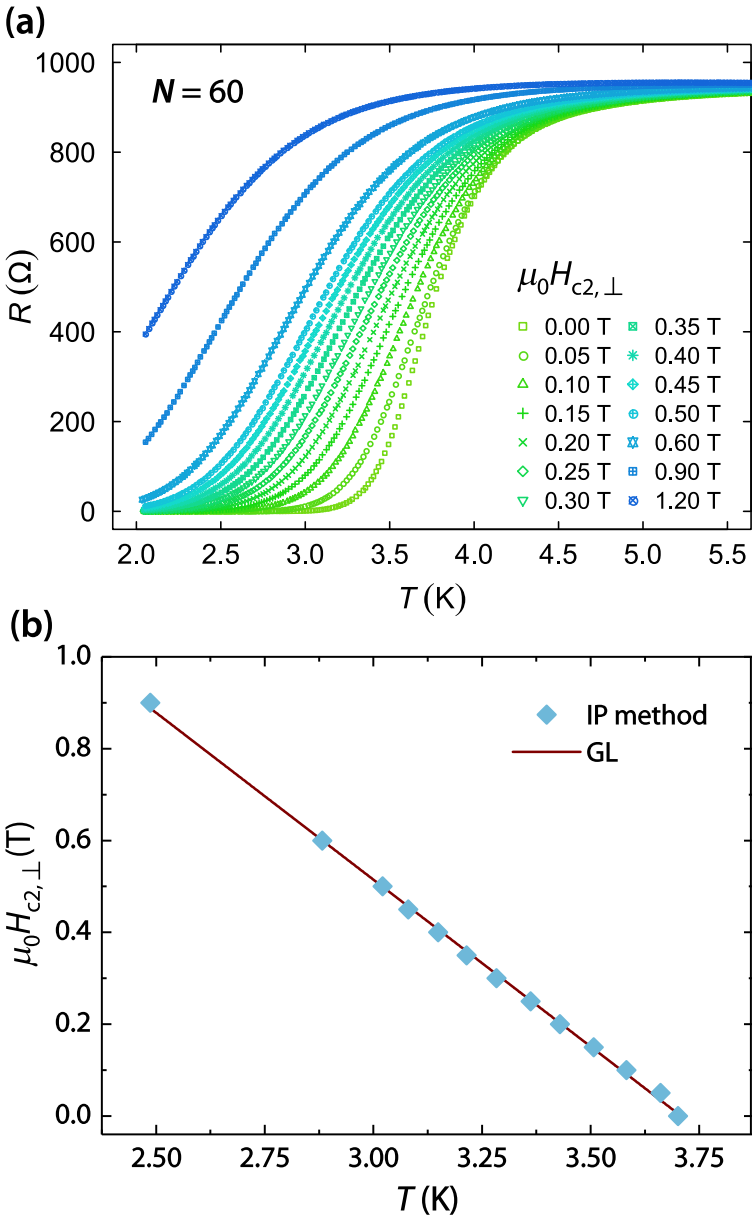

FIG. S5. Evaluation of the GL coherence length in a BBO/BPO BL with $N = 60$. a) Dependence of the resistance on the temperature at various magnetic fields applied perpendicular to the sample plane. The value of $H_{c2,\perp}$ is identified at the inflection point (IP) of the magneto-transport curves. b) Dependence of the upper critical magnetic field $H_{c2,\perp}$ as a function of temperature. Using $H_{c2,\perp}(T) = \frac{\phi_0}{2\pi\xi_{GL}^2}(1 - T/T_c)$ the coherence length is calculated to $\xi_{GL} = 11.0\,\text{nm}$. Using the same criteria for the evaluation of $H_{c2,\perp}$ of 95% of the normal-state resistance as explained in detail in Fig. S3 the coherence length is calculated to 9.6 nm.